applied sciences

MDPI

Article

Study on a Laser-Resistant Coating's Protective Effect on 7075 Aluminum Alloy

Shaozun Hong, Qi Pu, Xiaodong Jia * and Xin Cao

High Speed Aerodynamics Institute, China Aerodynamics Research and Development Center, Mianyang 621000, China; hongshaozun@163.com (S.H.)
* Correspondence: jiaxiaodong@cardc.cn

Abstract

To improve the laser-induced damage resistance of 7075 aluminum alloy, a typical aerospace material, a laser-resistant coating material for the surface of 7075 aluminum alloy was prepared in this paper. The performance of 7075 aluminum alloy coated with this coating was analyzed and tested by combining numerical simulation and experimental verification. The test results show that under the same laser irradiation conditions and geometric dimensions, the breakdown time of 7075 aluminum alloy coated with the laser-resistant coating is prolonged by 541.6%, and its laser-induced damage resistance is significantly improved.

Keywords: laser irradiation; laser damage; numerical simulation; coating material

1. Introduction

With the rapid development of laser weapon technology, the demand for laser irradiation protection of aerospace materials is increasingly urgent [1–5]. Studies have shown that under laser irradiation, metallic materials will experience temperature rise, melting, vaporization, spattering and other phenomena; while non-metallic materials may suffer from sublimation, chemical reactions, coking, exfoliation and other problems, eventually leading to structural failure [6,7]. At present, the main protection method to solve this problem is to coat functional coatings on the target surface to improve the laser-induced damage resistance. In terms of functional characteristics, existing coatings can be divided into four categories: reflective, ablative, thermal insulating and composite [8]. In recent years, high-reflectivity materials have attracted much attention due to their excellent laser protection performance. Such materials effectively reflect laser energy, making the energy acting on the substrate lower than the material damage threshold, thus achieving effective protection of the substrate and becoming a research focus of current laser protection materials [9,10]. Numerous studies have demonstrated that high-reflectivity coatings play a vital role in laser-induced damage resistance: Zhu et al. investigated the laser ablation behavior of plasma-sprayed perovskite coatings and found that the temperature rise rate was significantly inversely proportional to the coating reflectivity, confirming the key role of reflectivity in laser protection [11]. Zheng et al. further studied the ablation characteristics of plasma-sprayed Ta_2O_5 coatings, indicating that coatings with low initial reflectivity could achieve a significant increase in reflectivity after laser irradiation [12]. In the development of new high-reflectivity coatings, Yang et al. prepared a novel laser protection coating using phenolic resin and zirconium dioxide as raw materials. When irradiated for 8 s at a laser power density of 1503 W/cm^2, the reflectivity increment of the coated surface reached

Received: 18 May 2026
Revised: 18 June 2026
Accepted: 22 June 2026
Published: 23 June 2026

the maximum (75.7%) [13]. Experiments showed that the excellent heat absorption and thermal conductivity of the coating enabled it to effectively resist high-intensity continuous laser irradiation. In addition, Yang et al. developed a laser ablation-resistant composite coating by coating a SiC whisker and ZrB_2 particle-reinforced ZrO_2 sol-gel coating on an aluminum alloy substrate. After irradiation for 10 s at a laser power density of 6.3 kW/cm^2, the backside temperature of the substrate was only 150 °C [14].

Given that the study of ablation effects is an important part of evaluating the performance of protective coatings [15], this paper takes 7075 aluminum alloy, a typical aerospace material, as the substrate, coats a high-reflectivity laser-resistant coating on its surface, systematically studies its damage characteristics under continuous laser irradiation, and comprehensively analyzes its protective performance by combining numerical simulation and experimental verification.

2. Coating Design and Fabrication

2.1. Coating Design

To achieve a high damage threshold and superior stability of target materials under high-power laser irradiation, the material selection principle for laser-resistant coatings is established, namely combining high reflectivity with high thermal conductivity. Guided by this principle, we systematically carry out the design and selection of coating materials from multiple dimensions, including material physical mechanisms, laser protection performance, and process feasibility.

First, a candidate material database was constructed, focusing on metals with high reflectivity or excellent thermal conductivity such as Cr, Ni, Ag, and Au. Combined with the relevant literature [16,17], modeling and calculations were performed on the optical constants, thermal diffusion properties and material stability of these metals at the 1080 nm laser band. On this basis, small-scale sample deposition and thermal response tests were carried out to preliminarily evaluate the laser resistance potential of each material. Second, to fully account for the thermophysical compatibility, interfacial stability and deposition process adaptability between the coating and the aluminum alloy substrate, coupled simulation analyses were conducted on various material combinations to screen out material systems with more balanced performance and more stable structures. Finally, composite materials mainly composed of copper, silver and zinc were selected as coating constituents. Among them, Cu endows the coating with ultra-high thermal conductivity and favorable ductility, enabling rapid diffusion of laser energy and reduction of local temperature rise. Ag effectively boosts the reflectivity of the coating and cuts down the absorption of laser energy. Zn markedly lowers the coating density to realize lightweight design as much as possible, while improving the uniformity of thermal diffusion.

This alloy material exhibits favorable reflectance in the visible to near-infrared band, and its optical reflectivity can reach up to 95%, especially near the laser wavelength of 1080 nm. Benefiting from this property, the coating can reflect most of the incident laser energy, effectively restrain the laser energy absorption of the target substrate, and drastically mitigate thermal accumulation and ablation risk on the target surface.

2.2. Coating Fabrication

A variety of mainstream techniques are available for the fabrication of metallic coatings, including physical vapor deposition (PVD), chemical vapor deposition (CVD), electroplating/electroless plating, thermal spraying, cold spraying and air spraying. Nevertheless, each technique possesses distinct merits and drawbacks in practical engineering applications [18–21].

For instance, chemical vapor deposition is capable of producing high-quality coatings, yet it suffers from high production costs and low deposition rates. It cannot realize rapid processing of coated targets and interlayer targets within a short period, which imposes obvious restrictions on mass production and fast coating fabrication. Electroplating and electroless plating feature relatively simple operation, whereas they are subject to severe limitations in coating thickness and uniformity. Uniform coating thickness cannot be guaranteed on targets with diverse shapes and sizes, which will cause inconsistent coating performance and degrade the overall laser resistance of the substrate target. Cold spraying imposes strict plastic deformation requirements on coating feedstock; only highly ductile materials can be deposited via this approach. This greatly narrows the range of available coating materials and fails to satisfy specialized performance demands such as high reflectivity and superior thermal conductivity. By contrast, air spraying boasts easy operation and low cost, but the resultant coatings exhibit weak bonding strength with the aluminum substrate. The coating layer tends to peel off during service, which severely impairs the protective performance and service life, making it incapable of meeting the requirements for high-reliability laser-resistant coatings.

In summary, after comprehensively evaluating the advantages and disadvantages of various coating preparation methods, thermal spraying was ultimately selected as the processing technique for coated targets. Compared with conventional coating deposition methods, thermal spraying technology presents prominent superiorities in multiple aspects.

Firstly, benefiting from the extremely high temperature and energy density of plasma arcs, thermal spraying delivers a high deposition efficiency, enabling rapid coating fabrication and accommodating the processing requirements of large-area workpieces with complex geometries. Secondly, the thermal load on the substrate during spraying is relatively controllable, and the substrate temperature generally remains low. This helps avoid phase transformation and deformation of the material microstructure, preserving the inherent mechanical properties of the workpiece. Furthermore, thermal spraying supports an extensive range of feedstock materials and can fabricate metallic, ceramic and even composite coatings to achieve a diverse set of outstanding functional performances. The thermal spraying process mainly consists of two stages: the fabrication of spherical feedstock powders and the deposition of the functional coating.

2.2.1. Fabrication of Spherical Feedstock Powders

Spherical feedstock powders can perfectly meet the stringent requirements of thermal spraying processes in terms of powder feeding stability, heat transfer efficiency and coating quality. Firstly, spherical particles possess excellent flowability, which ensures smooth and uniform powder transport within the powder feeding system and avoids clogging or pulsation issues frequently encountered with irregularly shaped powders—a prerequisite for stable spraying. Secondly, spherical particles absorb heat more evenly in the high-temperature plasma jet, enabling rapid and consistent melting. This delivers high deposition efficiency and produces premium coatings featuring dense microstructure, low porosity and strong interfacial bonding strength. In contrast, irregular powders exhibit poor flowability that leads to uneven powder delivery, accompanied by non-uniform heating and melting inside the flame jet. Consequently, the resultant coatings tend to contain defects with reduced bonding strength, failing to guarantee reliable coating performance.

The preparation of spherical feedstock powders starts with high-purity metallic raw materials. To guarantee precise chemical composition of the final product, all raw materials are accurately weighed according to the designed mass ratio in the first step. Afterwards, the weighed raw materials are melted in a vacuum induction furnace. The furnace chamber is evacuated to a high vacuum level on the order of 10^{-3} Pa to eliminate oxygen and

water vapor to the greatest extent, creating a contamination-free melting atmosphere. Subsequently, melting is performed at 1000 °C under the shielding of high-purity argon inert gas. The melting temperature is precisely regulated to not only fully melt the high-melting-point Cu and facilitate its uniform diffusion but also minimize the holding duration at high temperature so as to effectively suppress the volatilization loss of Zn. After melt refining, the molten alloy is held at constant temperature for 3–5 h to achieve sufficient diffusion and homogenization of alloying elements, yielding a chemically homogeneous alloy melt. Once a uniform alloy melt is obtained, inert gas atomization is adopted to break up the liquid metal and rapidly solidify it into fine powders. In this process, the molten alloy stream is guided into an atomizing nozzle, while high-pressure inert gas ranging from 0.5 to 2 MPa is simultaneously injected. The high-velocity gas jet shatters the continuous liquid metal stream into numerous tiny droplets. As these droplets fall, surface tension spontaneously drives them to contract into spherical shapes, followed by rapid solidification within the cooling zone of the atomization tower. This technique produces powders with favorable sphericity. Strict control over atomization temperature and gas flow rate is implemented to mitigate element burning loss. The as-prepared powders are subjected to precision sieving to screen particles within a targeted size range of 15–45 μm. Finally, the classified powders are sealed and packaged under an inert gas atmosphere to avoid oxidation during storage.

2.2.2. Coating Spraying Process

Coatings were deposited on the substrate surface using a Praxair Model 5500 atmospheric plasma spraying system, which mainly consists of an integrated automatic control unit and a plasma spray gun. The integrated automation system comprises an exhaust ventilation unit, a gas purification unit, an ABB six-axis robotic manipulator, and a spraying control system. The spray gun adopted is the SG100 model manufactured by Praxair TAFA. The ABB six-axis manipulator was programmed to regulate the travel path, moving speed of the gun, and standoff distance between the gun nozzle and specimens. A Model 1264 volumetric powder feeder delivered the alloy feedstock powder into the plasma gun. In terms of process parameter configuration, key variables including plasma gas composition, arc current, powder feeding rate, standoff distance and substrate preheating temperature were systematically optimized according to the compatibility between powder characteristics and the substrate alloy.

By adjusting the arc current and gas mixture ratio, the feedstock particles can be fully heated and melted, then accelerated at high velocity toward the substrate surface to form dense coatings with strong interfacial adhesion. Meanwhile, precise control over powder feeding rate and standoff distance guarantees stable spraying operation and high deposition efficiency, thereby improving the homogeneity and consistency of the resultant coating. After deposition, comprehensive characterizations were performed to evaluate coating thickness, bonding strength and overall quality, eliminating defects such as weak adhesion and inhomogeneous microstructure.

3. Numerical Simulation Model and Parameter Settings

3.1. Software Introduction

The numerical simulation in this paper adopts COMSOL Multiphysics® v. 5.8 software, a powerful multiphysics field simulation software widely used in thermal, electromagnetic, structural, acoustic, fluid and other fields, with significant advantages, especially in dealing with complex coupling problems.

In laser simulation, COMSOL supports the accurate construction of Gaussian heat source models and can define the heat flux distribution towards the target surface according

to laser power, spot radius and spatial distribution. Compared with traditional software, COMSOL can not only conveniently express laser input in the form of a Gaussian function but also conduct detailed modeling of laser energy changes with time, space or material response through custom expressions, which is especially suitable for the analysis of laser transient heating, periodic pulse loading and multi-pulse cumulative effects.

3.2. Thermal Model

The thermal model describes the heat conduction process inside the material after laser energy input, which is the basic part of the entire thermo-mechanical coupling analysis. Considering the temporal variation and spatial inhomogeneity during laser irradiation, a transient heat conduction model combined with Gaussian heat source input is used to construct the real thermal loading boundary.

The heat conduction process follows Fourier's law, and its governing equation is:

$$\rho C_P \frac{\partial T}{\partial t} = \nabla \cdot (k \nabla T) + Q \quad (1)$$

In the equation, ρ is the material density, C_P is the specific heat capacity, k is the thermal conductivity, T is the temperature, t is the time, and Q is the heat source term representing the energy input per unit volume. Under laser loading, Q is converted from the heat flux on the target surface and applied to the material surface in the form of boundary heat flux.

To accurately reflect the spatial distribution characteristics of the laser beam, the heat source term is defined by a two-dimensional Gaussian distribution function, expressed on the target surface as:

$$q(r) = \frac{2P}{\pi R^2} exp(-2\frac{r^2}{R^2}) \quad (2)$$

where P is the total laser power, R is the laser spot radius, and r is the radial distance from the laser incident center. This heat flux is applied to the upper surface of the material and acts continuously with time to simulate the continuous laser irradiation process.

3.3. Geometric Model

The geometric model is constructed for two types of targets: a 7075 aluminum alloy target and a 7075 aluminum alloy target coated with a laser-resistant coating to compare their thermo-mechanical response differences. To simplify the simulation calculation, the model adopts a two-dimensional structure taken from the central section of the circular target, and the corresponding geometry is built in the software with boundary conditions applied.

The 7075 aluminum alloy target model is a single-material circular target with a diameter of ∅110 mm and a thickness of 3 mm. The 7075 aluminum alloy target model coated with laser-resistant coating is based on a 7075 aluminum alloy substrate with a diameter of ∅110 mm and a thickness of 2.95 mm, coated with a 50 μm thick laser-resistant coating, keeping the overall geometric dimensions consistent with the 7075 aluminum alloy target model. The contact condition between the laser-resistant coating and the substrate is set as perfect contact.

3.4. Boundary Setting Method and Basis

In the thermo-mechanical coupling simulation model, for thermal boundary conditions, the laser heat source is applied to the top surface of the geometric model through Gaussian distribution heat flux, whose spatial distribution follows the mathematical description of the Gaussian function, consistent with the energy distribution characteristics of the actual laser beam. Considering the transient characteristics of laser action and the

dominant effect of high-energy input, the influence of convection and radiation is ignored, and all boundaries except the laser loading surface are set as adiabatic conditions.

For mechanical boundaries, a free displacement constraint strategy is adopted, that is, no external fixed constraint is applied to the entire target, aiming to eliminate the interference of boundary conditions on the local stress field and purely present the inherent thermal stress distribution caused by the temperature gradient. The stress field is generated through the thermal expansion constitutive relation.

3.5. Software Parameter Settings

In the numerical simulation, the total laser power is set to 8 kW, the laser spot radius is 1.5 cm, and the laser action time is 30 s. Given that this simulation focuses on the thermo-mechanical response under instantaneous laser action with a short laser duration, constant physical parameters of each material at room temperature are adopted in the simulation to improve the stability and simplicity of model calculation, ignoring the influence of temperature on the thermophysical and mechanical properties of materials. The relevant material property parameters involved are shown in Table 1. Among them, the relevant parameters of 7075 aluminum alloy are derived from references [22], while those of the laser-resistant coating are obtained via laboratory tests.

Table 1. Material property parameters.

Items	7075 Aluminum Alloy	Laser-Resistant Coating
Density (kg/m^3)	2810	10,000
Thermal conductivity (W/m·K)	160	400
Specific heat capacity (J/kg·K)	960	200
Thermal expansion coefficient (1/K)	23.5×10^{-6}	19×10^{-6}
Young's modulus (GPa)	69	83
Poisson's ratio	0.33	0.37
Melting temperature (°C)	635	1000
Latent heat of fusion (J/kg)	3.5×10^5	2×10^5
Vaporization temperature (°C)	2000	2000
Latent heat of vaporization (J/kg)	1×10^7	8×10^6
Laser absorptivity (for 1080 nm laser)	25%	5%

For solution parameter settings, considering the short laser loading time and drastic temperature field change, the simulation adopts a transient multiphysics field coupling solution, using the software's built-in automatic time step control and BDF implicit time integration method to ensure a stable solution in the nonlinear region. The overall time interval is set to 30 s, and the calculation step is set to 0.2 s.

4. Test Conditions and Methods

4.1. Test Equipment and Working Conditions

The equipment used for the laser irradiation test mainly includes a fiber laser, a beam expander system, a laser power meter, a high-speed camera, a supplementary light source, a thermocouple and a temperature dynamic acquisition system matched with a thermocouple.

To better compare the laser-induced damage resistance of 7075 aluminum alloy before and after coating with laser-resistant coating, on the one hand, variables are strictly controlled to ensure the consistency of laser action conditions and target geometric dimensions; on the other hand, three repeated tests are carried out for both test materials to reduce random errors. The test optical path and equipment layout are shown in Figure 1.

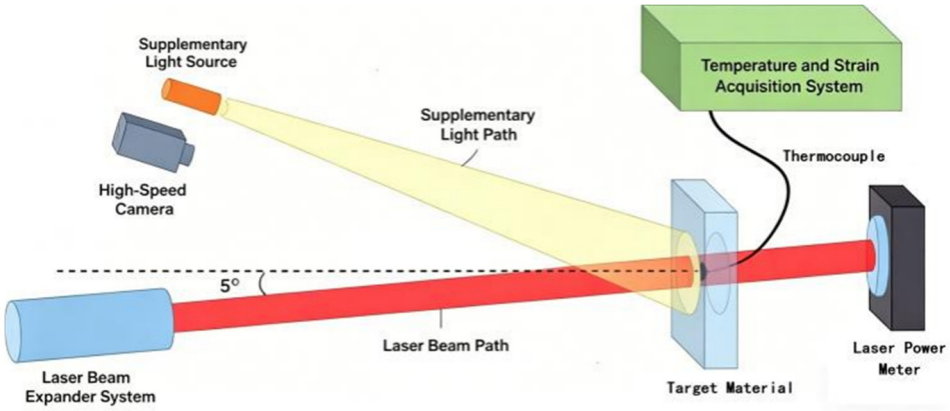

Figure 1. Schematic diagram of optical path and equipment layout.

To prevent the reflected light from the laser from damaging the laser, the laser incident angle is set to 5°. Detailed experimental parameters are presented in Table 2.

Table 2. Design of experimental conditions.

No.	Target Material	Laser Power	Laser Beam Radius	Target Thickness	Label
1	7075 Aluminum alloy	8 kW	1.5 cm	3 mm	A1
2	7075 Aluminum alloy	8 kW	1.5 cm	3 mm	A2
3	7075 Aluminum alloy	8 kW	1.5 cm	3 mm	A3
4	7075 Aluminum alloy with coating	8 kW	1.5 cm	3 mm	C + A1
5	7075 Aluminum alloy with coating	8 kW	1.5 cm	3 mm	C + A2
6	7075 Aluminum alloy with coating	8 kW	1.5 cm	3 mm	C + A3

4.2. Test Method

In the test, the damage process of the target during laser irradiation, the temperature change at the center of the target's back surface, and the breakdown time of the target were obtained.

Since the center of the target shows a state of high brightness and molten material spattering at the moment of breakdown, to more accurately obtain the target breakdown time, a combination of high-speed camera images, thermocouple-measured temperature and power meter-measured values is used to judge the target breakdown time. The judgment method of the thermocouple-measured temperature for target breakdown time is as follows: When the target is broken down, the thermocouple is directly irradiated by laser, and the temperature instantly exceeds the thermocouple range, resulting in an abnormal jump in the measured temperature. The time when this phenomenon occurs is taken as the target breakdown time. The judgment method of the power meter-measured value for target breakdown time is as follows: Start the power meter and collect data at the same time as the laser emits light. When the target is broken down, the power meter will receive the light and show a measured reading. The time when the power meter starts to show a reading is taken as the target breakdown time.

5. Result Analysis

5.1. Numerical Simulation Results

The numerical simulation results of the 7075 aluminum alloy target are shown in Figure 2.

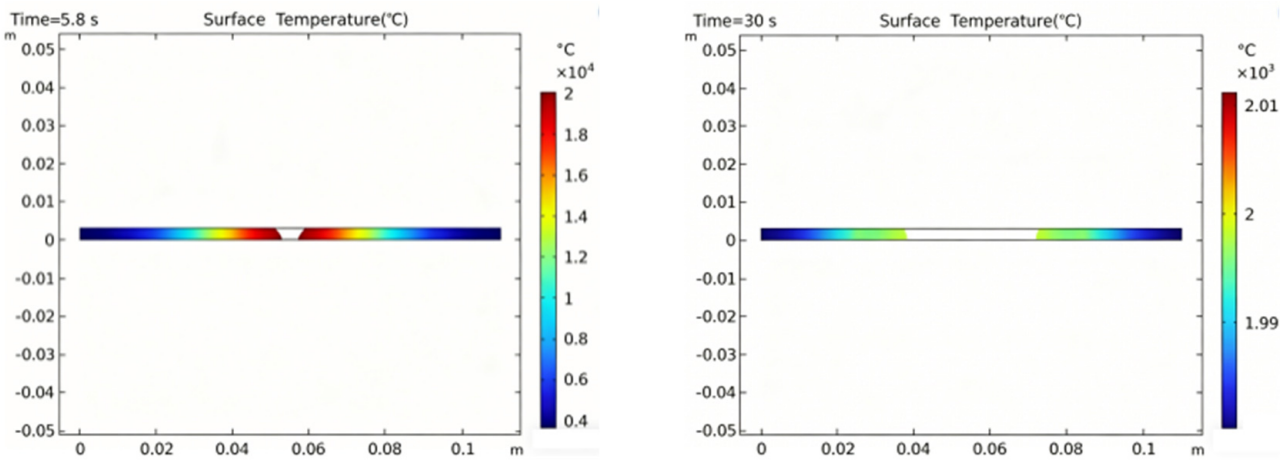

(**a**) t = 5.8 s (**b**) t = 30.0 s

Figure 2. Numerical simulation results of 7075 aluminum alloy target.

The results show that the 7075 aluminum alloy target is broken down after 5.8 s of laser irradiation, and the breakdown aperture increases with time until it approaches the laser beam diameter.

The numerical simulation results of the target coated with laser-resistant coating are shown in Figure 3.

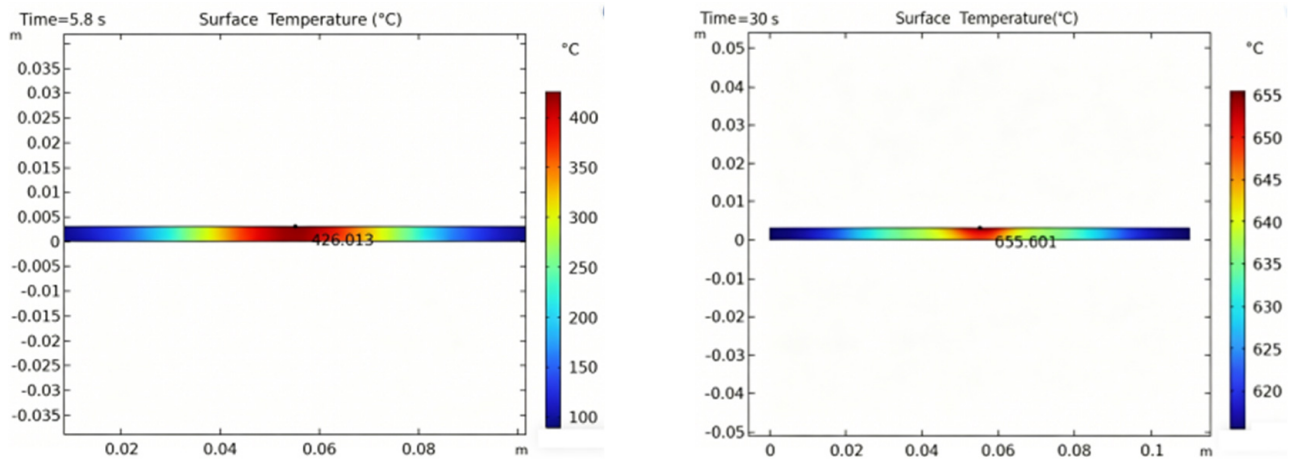

(**a**) t = 5.8 s (**b**) t = 30.0 s

Figure 3. Numerical simulation results of target coated with laser-resistant coating.

The results show that after 5.8 s of laser irradiation, the maximum temperature of the 7075 aluminum alloy target coated with laser-resistant coating is about 426 °C, and after 30 s of irradiation, the maximum temperature of the target only reaches about 656 °C, close to the melting point of 7075 aluminum alloy, without breakdown, indicating that the laser-resistant coating has a good protective effect.

5.2. Test Results

From the images captured by the high-speed camera in the test, shown in Figures 4–6, under the action of laser irradiation, the surface of the 7075 aluminum alloy target gradually melts and bulges with the increase in temperature, then the bulge ruptures, molten material spatters, and the target is broken down. It can be seen from the images that the initial melting times of the target surface are 1.2 s, 1.2 s and 1.1 s, respectively, and the breakdown times are 4.0 s, 4.3 s and 4.1 s, respectively.

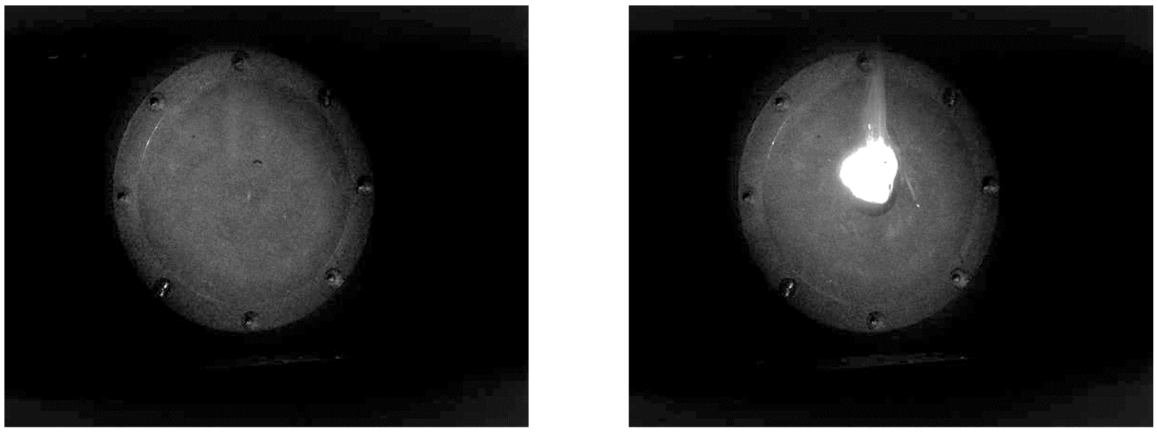

(**a**) Initial surface melting (t = 1.2 s) (**b**) Breakdown moment (t = 4.0 s)

Figure 4. High-speed camera shooting results of the first target of 7075 aluminum alloy.

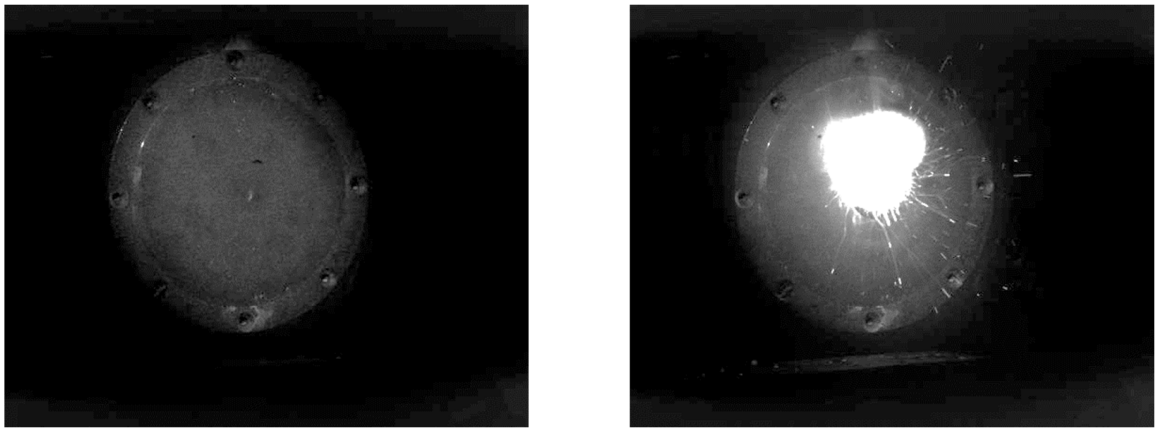

(**a**) Initial surface melting (t = 1.2 s) (**b**) Breakdown moment (t = 4.3 s)

Figure 5. High-speed camera shooting results of the second target of 7075 aluminum alloy.

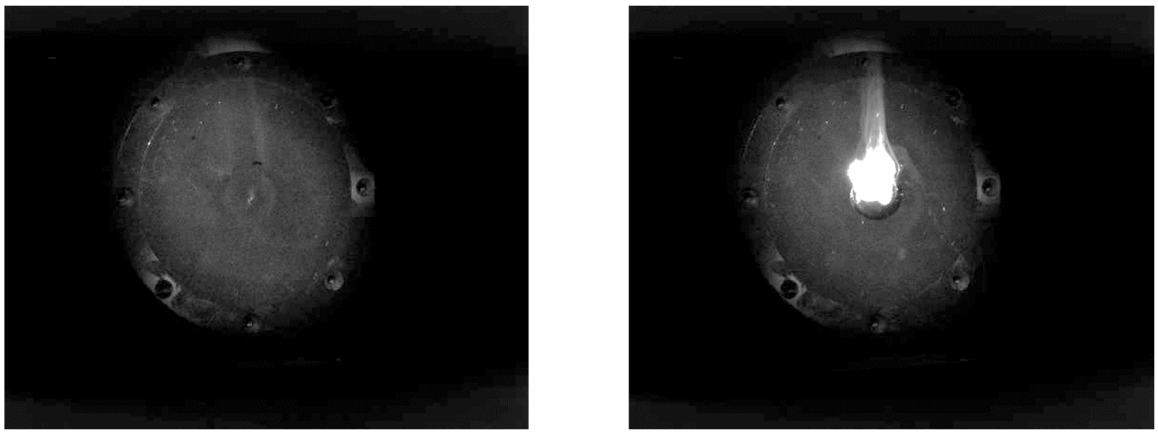

(**a**) Initial surface melting (t = 1.1 s) (**b**) Breakdown moment (t = 4.3 s)

Figure 6. High-speed camera shooting results of the third target of 7075 aluminum alloy.

As shown in Figures 7–9, after coating with laser-resistant coating, the target surface shows no reaction for a long time under laser irradiation. With the deposition of laser energy, the coating material on the target surface begins to melt and glow, followed by molten material spattering and target breakdown. The test results show that the initial melting times of the target surface coated with laser-resistant coating are 25.0 s, 25.1 s and 23.1 s, respectively, and the breakdown times are 27.2 s, 27.2 s and 25.1 s, respectively.

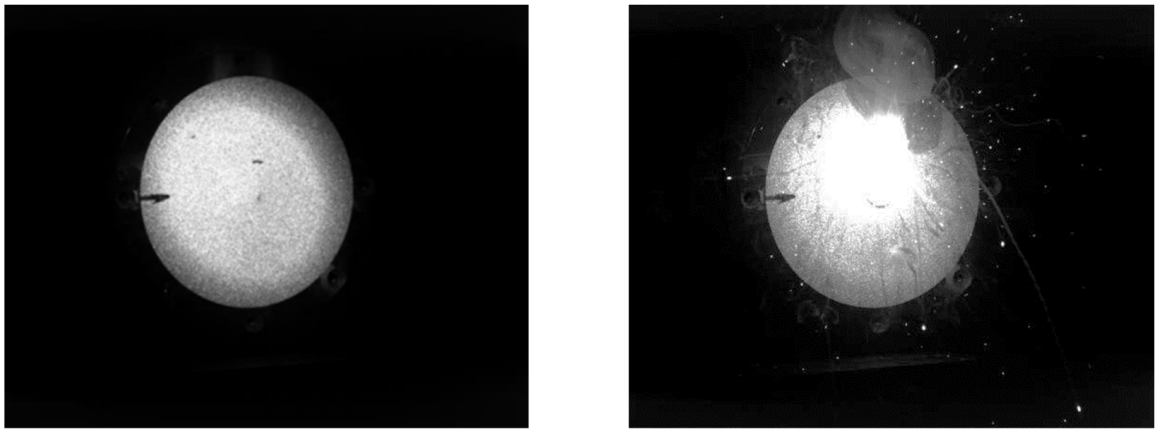

(**a**) Initial surface melting (t = 25.0 s) (**b**) Breakdown moment (t = 27.2 s)

Figure 7. High-speed camera shooting results of the first target of 7075 aluminum alloy with coating.

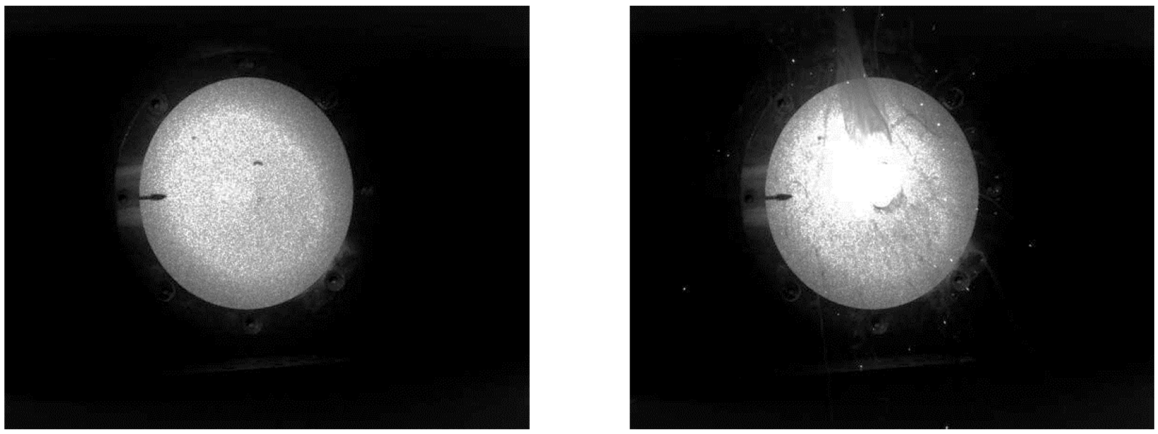

(**a**) Initial surface melting (t = 25.1 s) (**b**) Breakdown moment (t = 27.2 s)

Figure 8. High-speed camera shooting results of the second target of 7075 aluminum alloy with coating.

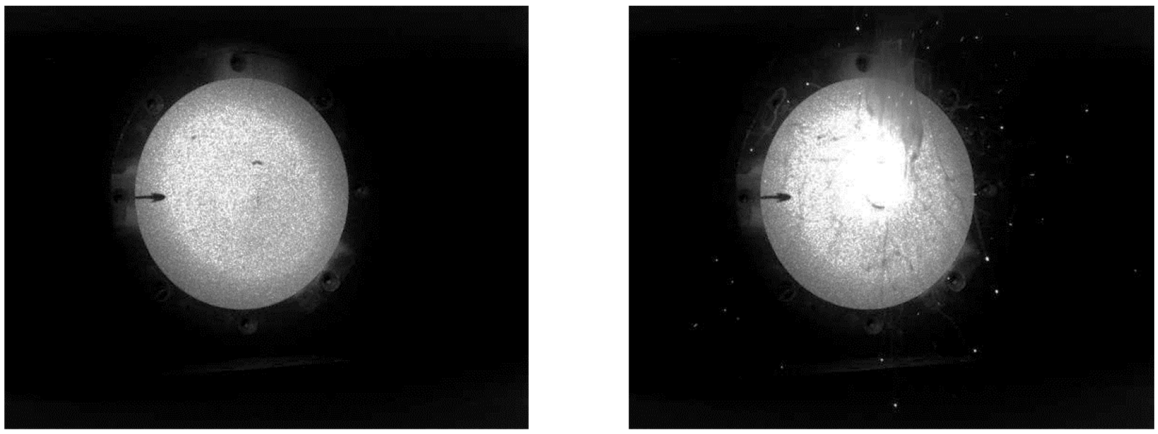

(**a**) Initial surface melting (t = 23.1 s) (**b**) Breakdown moment (t = 25.1 s)

Figure 9. High-speed camera shooting results of the third target of 7075 aluminum alloy with coating.

The temperature rise curve at the center of the target back surface measured by the thermocouple sensor is shown in Figure 10. According to the measurement results, the front surface temperature of the 7075 aluminum alloy target is transmitted to the back surface in about 2 s, and the back surface temperature rises rapidly, reaching the melting point of 7075 aluminum alloy in about 3.5 s, and an abnormal jump in temperature begins

to occur in about 4.5 s. For the target coated with a laser-resistant coating, the back surface also begins to receive the temperature transmitted from the front surface in about 2 s of laser action. Over time, the back surface temperature rises slowly and remains below 400 °C for a long time. Until about 27 s, an abnormal jump in the back surface temperature of the target occurs.

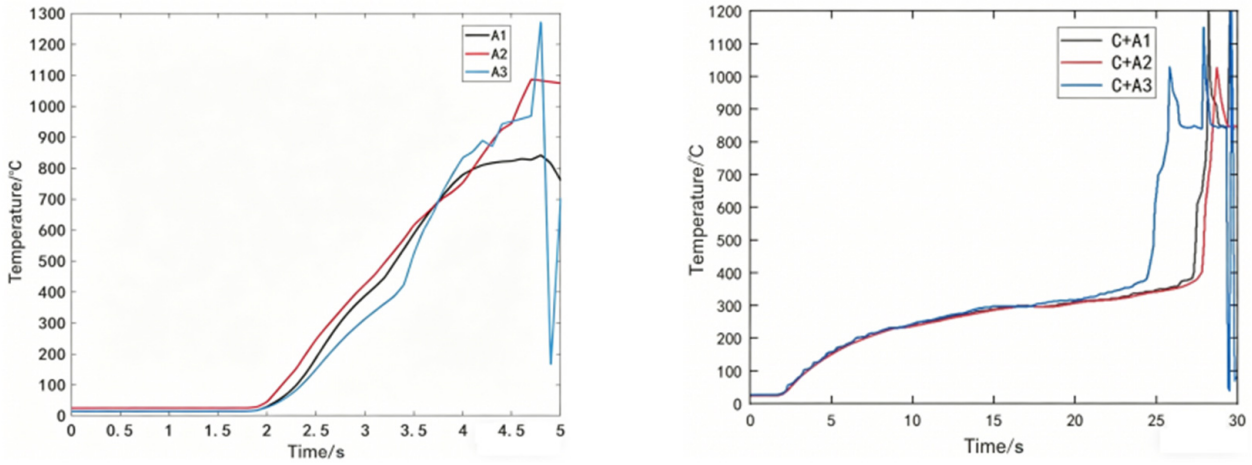

(**a**) 7075 Aluminum alloy target (**b**) Coating target

Figure 10. Thermocouple measurement results at the center of the target's back surface.

The power meter measurement results are shown in Figure 11. The results show that in the three tests of the 7075 aluminum alloy target, the power meter collects laser power at about 4 s; in the three tests of the target coated with laser-resistant coating, the power meter collects laser power at about 27 s in the first two tests and at about 25 s in the third test.

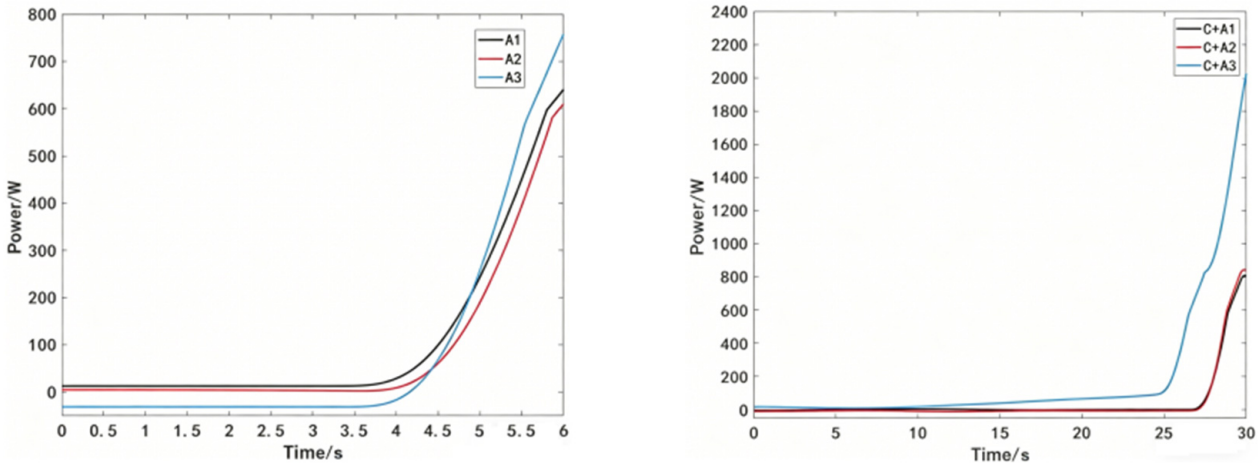

(**a**) 7075 Aluminum alloy target (**b**) Coating target

Figure 11. Laser power meter measurement results.

5.3. Comparative Analysis of Results

Combined with the aforementioned numerical simulation and test results, the breakdown time of the 7075 aluminum alloy target in the numerical simulation is slightly later than that in the actual test, and the laser-resistant coating target in the numerical simulation does not break down after 30 s of laser irradiation, while the actual test target breaks down in about 25 s, showing a deviation between the numerical simulation and the actual test. Preliminary analysis may be caused by the following two reasons: on the one hand,

the material parameter settings in the numerical simulation tend to be idealized, and the surface condition, local coating composition and reflectivity of the target used in the actual test are different from those in the numerical simulation, resulting in result differences; on the other hand, the microstructure and mechanical properties of 7075 aluminum alloy will change after reaching the phase transition temperature, which is ignored in the numerical simulation, resulting in result differences. To better analyze the test results, the target breakdown times obtained by different methods in the test are further sorted out in Table 3.

Table 3. Summary of target breakdown time.

Test No.	Target Material	High-Speed Camera Result	Thermocouple Measurement Result	Power Meter Measurement Result
1	7075 aluminum alloy	4.0 s	4.7 s	4.0 s
2		4.3 s	4.5 s	4.0 s
3		4.1 s	4.6 s	3.8 s
4	7075 aluminum alloy with coating	27.2 s	27.3 s	27.0 s
5		27.2 s	27.5 s	27.0 s
6		25.1 s	25.0 s	25.0 s

From the average value of target breakdown time obtained by three different measurement methods, there are slight deviations among the three methods, with the maximum deviation of only 0.67 s, all of which can effectively judge the target breakdown time. Taking the high-speed camera shooting results as the main reference, the average breakdown time of the 7075 aluminum alloy target is 4.13 s, while that of the target coated with laser-resistant coating is 26.5 s, prolonged by 541.6%. Based on this, it can be concluded that the laser-resistant coating has a good protective effect.

6. Conclusions

Numerical simulation and test results show that the laser-resistant coating prepared in this paper exhibits significant performance on the surface of 7075 aluminum alloy, prolonging the breakdown time of the material under the same laser action conditions by 541.6%, effectively enhancing the laser-induced damage resistance of the material, and has good application potential and development value. In the future, the laser protection performance of the laser-resistant coating in complex environments will be further improved, and the application scenarios will be expanded through continuous optimization of the preparation process and material formula, providing more comprehensive technical solutions for different fields.

Author Contributions: Conceptualization, S.H. and X.J.; methodology, S.H.; validation, S.H., Q.P. and X.C.; resources, X.J.; data curation, Q.P.; writing—original draft preparation, S.H.; writing—review and editing, X.J.; visualization, S.H. All authors have read and agreed to the published version of the manuscript.

Funding: This research received no external funding.

Data Availability Statement: Dataset available on request from the authors.

Conflicts of Interest: The authors declare no conflict of interest.

References

1. Cheng, L.; Tong, Z.C.; Liu, W.J. Present status and tendency of foreign laser weapo. *Shipboard Electron. Countermeas.* **2019**, *42*, 56–58. [CrossRef]
2. Ahmed, S.A.; Mohsin, M.; Ali, S.M.Z. Survey and technological analysis of laser and its defense applications. *Def. Technol.* **2021**, *17*, 583–592. [CrossRef]

3. Karr, T.; Trebes, J. The new laser weapons. *Phys. Today* **2024**, *77*, 32–38. [CrossRef]
4. Yang, J.; Zong, S.; Chen, L. Developments and trends of laser weapons. *Laser Infrared* **2021**, *51*, 695–704. [CrossRef]
5. Zhu, J.P.; Ma, Z.; Gao, L.H.; Liu, Y.B.; Wang, F.C.; Liu, L.; Zhu, S.Z. Research on reflective laser protective coating based on plasma spraying. *Chin. Opt.* **2017**, *10*, 578–587. [CrossRef]
6. Li, S.W.; Wu, L.F.; Yang, G.J.; Chen, L. Preparation and protective performance of high-reflection and high-thermal insulation laser protection coatings. *Mater. Prot.* **2024**, *57*, 84–95. [CrossRef]
7. Wang, H.Q.; Zhao, Y.F.; Teng, T.; Zhao, Y.; Wang, X.; Lu, K.; Fan, S.; Liu, Y.; Yin, F. Research progress of laser protective materials and their applications in coatings. *Chin. Surf. Eng.* **2022**, *35*, 51–72. [CrossRef]
8. Zheng, J.Y.; Ma, Z.; Gao, L.H. Development of intelligent anti-high power laser materials. *Adv. Ceram.* **2020**, *41*, 121–133. [CrossRef]
9. He, H.B.; Hu, H.Y.; Tang, Z.P.; Fan, Z.X.; Shao, J.D. Laser-induced damage morphology of high-reflective optical coatings. *Appl. Surf. Sci.* **2005**, *241*, 442–448. [CrossRef]
10. Li, S.Y.; Zhang, X.L.; Zhang, K.X.; Xu, H.; Zhao, J.; Pan, L.; Li, Y. Research progress on the application of laser protection of highly reflective ceramic coating materials. *Flight Control Detect.* **2025**, *8*, 12–19. [CrossRef]
11. Zhu, J.; Ma, Z.; Gao, Y.; Gao, L.; Pervak, V.; Wang, L.; Wei, C.; Wang, F. Ablation behavior of plasma-sprayed $La_{1-x}Sr_xTiO_{3+\delta}$ coating irradiated by high-intensity continuous laser. *ACS Appl. Mater. Interfaces* **2017**, *9*, 35444–35452. [CrossRef] [PubMed]
12. Zheng, J.; Wen, K.; Liu, Y.; Gao, L.; Ma, Z.; Diao, X. Laser irradiation behavior of plasma-sprayed tantalum oxide coatings. *Ceram. Int.* **2020**, *46*, 3875–3881. [CrossRef]
13. Yang, Z.; Zhang, L.; Zhang, Y.; Guo, X.; Chen, K.; Lu, K.; Zhang, J. Reflection and thermal characteristics of a novel reflective phase-change coating irradiated by high-power continuous laser. *Ceram. Int.* **2022**, *48*, 11365–11377. [CrossRef]
14. Yang, M.; Wang, T.; Wu, M. Ablation behavior of SiC whisker and ZrB_2 particle-filled ZrO_2 sol-gel composite coating under high-intensity continuous laser irradiation. *Ceram. Int.* **2021**, *47*, 26327–26334. [CrossRef]
15. Cheng, Y.; Zhu, M.Z.; Ma, Y.F.; Wei, J.; Liu, X.; Ding, F.; Tan, C.; Chen, X.; Guo, Y.; Chu, H. Mechanism and effects of complex laser ablation. *Infrared Laser Eng.* **2016**, *45*, 1105005. [CrossRef]
16. Wellershoff, S.S.; Hohlfeld, J.; Güdde, J.; Matthias, E. The role of electron-phonon coupling in femtosecond laser damage of metals. *Appl. Phys. A* **1999**, *69*, S99–S107. [CrossRef]
17. Yang, P.L.; Wu, Y.; Zhang, L.; Feng, G.; Zhao, J. Reflective Properties of Diffuse Gold Film at 1.064 μm under High-Power Laser Irradiation. *Chin. Opt.* **2019**, *12*, 913–919. [CrossRef]
18. Dan, A.; Bijalwan, P.K.; Pathak, A.S. A review on physical vapor deposition-based metallic coatings on steel as an alternative to conventional galvanized coatings. *J. Coat. Technol. Res.* **2022**, *19*, 403–438. [CrossRef]
19. Wang, R.X.; Wang, H.Y.; Xue, S.; He, J.; Chen, Q.; Zhang, Q.; Xie, P.; Yang, W.; Tan, J. Research progress of chromium-based thin film deposition technology on inner surface of tubular workpieces. *J. Mech. Eng.* **2023**, *59*, 56–72. [CrossRef]
20. Liu, M.J.; Zhang, G.; Lu, Y.H.; Han, J.Q.; Li, G.R.; Li, C.X.; Li, C.J.; Yang, G.J. Plasma spray–physical vapor deposition toward advanced thermal barrier coatings: A review. *Rare Met.* **2020**, *39*, 566–582. [CrossRef]
21. Mehta, A.; Vasudev, H.; Singh, S.; Prakash, C.; Saxena, K.K.; Linul, E.; Buddhi, D.; Xu, J. Processing and advancements in the development of thermal barrier coatings: A review. *Coatings* **2022**, *12*, 1318. [CrossRef]
22. Rapid-Protos. 7075 Aluminum: Properties, Composition, and Applications of This High-Strength Aerospace Alloy. Rapid-Protos. 18 September 2025. Available online: https://www.rapid-protos.com/7075-aluminum-properties-composition-and-applications-of-this-high-strength-aerospace-alloy/#toc_Thermal_Properties_of_7075_Aluminum (accessed on 18 June 2026).